Caspian Journal of Applied Sciences Research, 1(11), pp. 71-82, 2012
Available online at http://www.cjasr.com
ISSN: 2251-9114, ©2012 CJASR

A Novel Method for Determination of Grinding Wheel Loading

Hamed Adibi[1], Seyed Mehdi Rezaei[2,*] , Ahmed Aly Diaa Mohammed Sarhan[3]

[1, 2]Department of Mechanical Engineering, Amirkabir University of Technology, Tehran, Iran
[1, 2]New Technology Research Center, Amirkabir University of Technology, Tehran, Iran
[1,3]Center of Advanced Manufacturing and Material Processing, Department of Engineering Design and Manufacture, Faculty of Engineering, University of Malaya, Kuala Lumpur, 50603, Malaysia
[3]Department of Mechanical Engineering, Faculty of Engineering, Assiut University, Assiut, 71516, Egypt
*Corresponding Author: smrezaei@aut.ac.ir

Wheel surface condition plays an important role in the grinding operation. Wheel loading which is chip accumulation in the space between grains leads to the deterioration of wheel cutting ability and causes excessive force and temperature. Identification of wheel loading is an important issue for optimizing the dressing intervals but it can be a time consuming and an expensive process. A novel technique based on digital image processing to determine the loading areas over the surface of CBN vitrified grinding wheels using the toolbox of MATLAB is presented in this paper. The optical characteristics of the metal chips, the abrasive grains and wheel bond are considered. Edge detection by means of Sobel method is applied to distinguish the wear flat area and chip metal loading debris. Morphological operations including dilation and erosion procedure are applied to process the image and calculate the ratios of the loading areas over the wheel surface. Experiments were performed to examine the repeatability of the proposed technique. The results were verified by the use of a scanning electron microscope.

Key words: Grinding, Wheel loading, Image processing.

1. INTRODUCTION

Due to the property of difficult-to-cut materials, grinding is one of the effective machining methods for superalloys (Zhong et al., 2001; Teichera et al., 2008). In grinding of such ductile materials, frequently removed chips may adhere into porosities between abrasive grains or weld on top of cutting grains which is called wheel loading (Liu et al., 2007; Cai et al., 2003). This phenomenon leads to dull wheel grains which results in increased rubbing and excessive vibration.

It raises the cutting force, temperature and reduces wheel life (Cameron et al., 2010). CBN vitrified grinding wheels provide an ideal solution for many applications because of the possibility of the wheel porosity and structure control in vitreous bonds (Teichera et al. 2008; Wei et al., 2010). However, this type of wheel is prone to loading particularly in grinding of superalloys (Liu et al. 2007; Zhong and Hung, 2000). Dressing operation must be applied optimally to prevent serious detrimental damage to workpiece along with improving of the wheel life. However for this kind of wheel, frequent dressing should be avoided as it is time consuming and expensive. Therefore, wheel condition must be monitored periodically. Most methods applied, monitor the grinding wheel condition and utilize a touch-trigger probe inspection. Sakamoto et al (1998) fitted a laser micrometer directly on the wheel head of a CNC surface grinder. Wheel loading was evaluated qualitatively by comparing the profile of wheel surface and micro-observation of the ground surface. Mokbel and Maksoud (2000) applied acoustic emission technique to monitor the condition of grinding wheel. The inherent sensitivity of acoustic-emission-based monitoring is a serious problem of this method. Srivastava et al applied X-Ray fluorescence technique for loading measurement (Srivastava et al., 1985). High energy was utilized by an X-Ray source to determine wheel loading in grinding of lead and mild-steel. Kim and Ahn used eddy current and laser displacement sensors to measure loading on the working wheel surface and the topography of the dressed wheel to decide a proper dressing interval (Kim and Ahn, 1999).

The most important limitation of these techniques is the cost of equipments. Other wheel monitoring techniques including chemical detection, calorimetry, spectroscopy, magnetization and radiotracing have been reported but are all time consuming and expensive processes (Mokbel and Maksoud, 2000 , Srivastava et al. 1985, Kim and Ahn, 1999, Mao et al., 2010 , Lauer-Schmaltz and Konig,1980, Dornfeld et al., 2003, Konig and Lauer-Schmaltz,1980). Today, machine vision and digital image processing have

benefited the industries that employ it. As long as computer processing speed continues to increase while the cost of storage memory continues to drop, the field of digital image processing will grow. These widespread applications include quality control in manufacturing (Mersmann, 2011), tool monitoring in machining processes (Castejon et al., 2007) surface roughness control (Al-Kindi and Shirinzadeh, 2007), wheel wear monitoring in grinding operation (Lachance et al., 2004; Yasui et al., 2001; Hosokawa and Yasui, 1996 ; Feng and Chen, 2007) and many others. Image processing had been applied for examining of grinding wheel surface condition by some researchers (Lachance et al., 2004, Yasui et al., 2001). (Yasui et al., (2001) developed a system for extracting the cutting edge of a grinding wheel for examination of the surface condition using Image processing technique and had been applied for calculating the cutting edge ratio. Feng applied this technique for surface condition monitoring of Al2O3 wheel (Feng and Chen, 2007). Lachance et al used image processing for the measurement of wear flat area of grinding wheels (Lachance et al., 2004). This method was developed with a new technique called region growing as a supplementary solution for the detection of wear flat areas. Although, scanning electron microscope (SEM) is one of the best ways for observation of wheel surface but it is very expensive and is not practical for automated measurement.

In this paper, a new technique based on image processing using Toolbox of MATLAB for chip loading identification on CBN vitrified wheel is presented. Due to fine chips and related loading debris in grinding with CBN wheels, a portable digital microscope with high resolution equipped with adjustable LED light source is applied. Light properties and optical characteristics of metal loaded debris, abrasive grains and vitreous bond were investigated to distinguish the chip loaded debris from others. Edge detection, image normalization, dilation and erosion process were applied to process the image to calculate the ratios of the loading areas over wheel surface. SEM observations were used to assess the outcome of this technique. Statistical analysis was used to obtain the number of required images. Experiments were also conducted to investigate the efficiency of the technique in term of repeatability.

2. PROPERTIES OF LIGHT

The optical properties of crystals are obtained using x-ray diffraction and direct chemical analyses. These properties are the most reliable tool available to distinguish and identify materials. The optical properties depend on the manner that visible light is transmitted through the crystal and thus are dependent on crystal structure, crystal symmetry, and chemical composition of the materials (Nelson, 2012). Light is electromagnetic radiation that has properties of waves. The electromagnetic spectrum can be separated into several bands founded on the wavelength of the light waves. Visible light represents a slender group of wavelengths between about 380 to 730 nm (Peatross and Ware, 2011). Human eyes interpret these wavelengths as special colors. If only a single wavelength come into the eyes, they are interpreted as a certain color. As shown in Fig.1, when light strikes an interface between two substances with different refractive indices, it will be reflected off the interface at the same entrance angle. Alternatively it will be transmitted through the substance with different refractive index which depends on the transparency of the substance (Peatross and Ware, 2011). The vitrified bond of the wheel contains glass compositions of alumina-silicate system. Abrasive grains are Cubic boron nitride which is synthesized at pressures above 4.5 GPa and temperatures above 1500 K (Dou et al., 2006). The light wavelength range which is transparent to SiO_2 is 0.2–4.5 μm. For Al_2O_3 this is 0.15– 6.5 μm, therefore Al_2O_3 and SiO_2 are relatively transparent to the visible light (Feng and Chen, 2007). Pure CBN is highly transparent or slightly amber and can transmit over 99% of the light with wavelengths in the range of 250-900 nm (Song et al., 2010; Eremets et al., 1995). Different colors can be produced depending on defects or an excess of boron (less than 1%) (Haines et al., 2001). Defects attributed to the effect of doping solvent-catalysts (i.e. Li, Ca, or Mg nitrides) with Al, B, Ti, or Si induces a change in the morphology and color of CBN crystals (Bocquillon et al., 1993). However, the CBN crystal is transparent and the clogged metal chips on the wheel cutting surface are opaque. Workpieces ground were Inconel 738 in this investigation. Therefore, when the light irradiates the CBN vitrified wheel surface, metal chips adhered on it reflect light robustly and appear brighter than other area as shown in Fig.2. Image processing technique applies this principle to calculate the amount of chip loaded over the wheel surface.

3. PROPERTIES OF LIGHT

The procedure of proposed image processing technique to analyze the captured image of the wheel surface can be categorized in three stages. Edge detection, Image segmentation and Morphological operations are described separately in the following sections.

3.1. Edge detection

Edge detection is the process of locating and identifying sharp discontinuities in an image. The discontinuities are sudden changes in pixel intensity which characterize boundaries of the object in an image. Edge detection has been used by object recognition, target tracking, segmentation, etc (Gonzalez et al., 2010). Several edge detection methods are in use. Beside this diversity, the majority of commonly used methods are alike. Derivative operators are applied on images and compute the gradient of several directions and combine the result of each gradient. The values of the gradient magnitude and orientation are estimated using differentiation masks. The magnitude of this derivative can be used to detect the presence of the edges. These several methods of edge detection include Sobel, Prewitt, Roberts, and Canny. Sobel which is a popular method was used in this work due to its simplicity and common uses. In addition, the Sobel operator holds a smoothing effect to reduce noise which is one of the reasons for its popularity (Gonzalez et al., 2010). Matlab contains various toolboxes like image toolbox that has many functions and algorithms. The function used in this work was Standard Sobel operator and includes the following steps.

Step 1: Convolution with gradient (Sobel) mask
Step 2: Magnitude of gradient.
Step 3: Thresholding.

First step is based upon a differentiation operator that approximates the gradient of the image intensity. As shown in Fig. 3, any point on the Cartesian grid has its eight neighbor's image intensity or pixel value. Technically, this differentiation operator using two convolutions (one horizontal and one vertical) with a minimal size kernel (3x3) to get local gradients from which the gradient magnitude can be computed. The directional derivative estimates vector G and was defined as intensity difference divided by distance to the neighbor. It is noted that the neighbors group into antipodal pairs: (a , i), (b , h), (c , g), (f , d). The vector sum for this gradient estimate is (Gonzalez et al., 2010):

$$G = \frac{(c-g)}{R}.\frac{[1,1]}{R} + \frac{(a-i)}{R}.\frac{[-1,1]}{R} + (b-h)[0,1] + (f-d)[1,0] \quad (1)$$

Where $R = \sqrt{2}$. This vector is obtained as

$$G = [(c-g-a+i)/2 + f - d, (c-g+a-i)/2 + b - h] \quad (2)$$

The resultant formula is given as follows (see, for detail (Gonzalez et al., 2010) :

$$G' = 2.G = [(c-g-a+i) + 2.(f-d), (c-g+a-i) + 2(b-h)] \quad (3)$$

The weighting functions according to Fig. 4 for x and y components were obtained by using the above vector. In the second step the magnitude of the derivative is calculated by the above masks. The values can be used to detect the presence of the edges of objects in the third step.

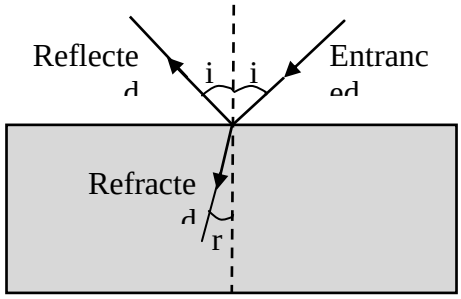

Fig. 1: Light striking between interface of different substance

3.2. Image segmentation

Image segmentation is a fundamental processing step for many image processing applications. There are many algorithms used for image segmentation. Some of them segment an image manually while others can segment automatically (Meyer, 1992). Several general purpose algorithms and techniques are available for image segmentation. These techniques often have to be combined with domain knowledge in order to effectively solve an image segmentation problem for a problem domain. The most common method of image segmentation is the threshold

technique. This method is based on a clip-level (or a threshold value) to turn a gray-scale image into a binary image. The key of this method is to decide on the threshold value. Several popular methods are used in industry including the maximum entropy method, Otsu's method (maximum variance), K-Means clustering and many others (Gonzalez et al., 2010, Meyer, 1992). During the thresholding process, individual pixels in an image are labeled as "object" if their pixel value are greater (or smaller) than threshold value. Other pixels are labeled as "background". Characteristically, an object pixel value is assigned "1" while a background pixel value is assigned "0." Finally, a binary image is created by coloring each pixel white or black, depending on a pixel's label. Several different methods for choosing a threshold exist. Users can manually choose a threshold value, or a thresholding algorithm can compute a value automatically. This is known as automatic thresholding. A sophisticated and more reliable approach might be to create a histogram of the image pixel intensities and use the valley point as the threshold. The histogram approach assumes that there is some average value for the background and object pixels. A typical gray scaled image of wheel surface is shown in Fig. 5. The histogram of pixel value along the line A – B is plotted in Fig. 5(b). The vertical axis of the graph represents the pixel value. The magnitudes of 0 and 255 correspond to black and white pixels, respectively. It is evident that the pixel values of metal loaded area are higher than 120 approximately. But the actual pixel values have some variation around these average values. However, this may be computationally expensive and it is difficult to select an accurate threshold. One method that is relatively simple and does not require any specific knowledge of the image was used in this work. It is also robust against image noise. The iterative method was used in this work is as follow:

(1) An initial threshold (T) is chosen; this can be done randomly. (It was chosen 120 according to histogram plot Fig. 5b in this study).

(2) The image is segmented into object and background pixels as described above, creating two sets:

$G_1 = \{f(m,n) \text{ if } f(m,n) > T\}$ (object pixels)

$G_2 = \{f(m,n) \text{ if } f(m,n) \leq T\}$ (background pixels) (note, f(m,n) is the value of the pixel located in the m^{th} column, n^{th} row)

(3) The average of each set is computed.

M_1 = average value of G_1

M_2 = average value of G_2

(4) A new threshold is created that is the average of M_1 and M_2

$T' = (M_1 + M_2)/2$

Step 2 is used again with a new threshold computed in step four. This is repeated until the new threshold matches the one before convergence was reached. This iterative algorithm is a special one-dimensional case of the K-means clustering algorithm, which has been proven to converge at a local minimum (Meyer, 1992).

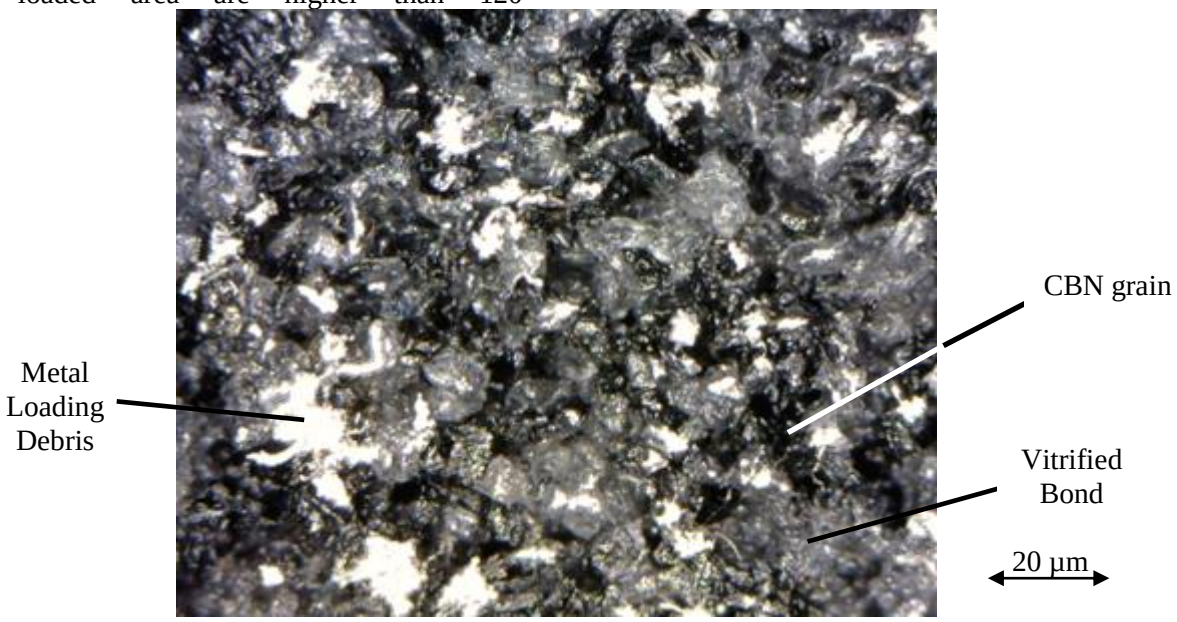

Fig. 2: CBN vitrified wheel surface image captured with digital microscope

3.3. Binary morphological operations

Morphology is a widespread set of image processing operations with process images based on shapes. In a morphological operation, the value of each pixel in the output image is based on a comparison of the corresponding pixel in the input image with its neighbors. The most basic morphological operations are dilation and erosion which were used in this work. In the morphological dilation and erosion operations, the state of any given pixel in the output image is determined by applying a rule to the corresponding pixel and its neighbors in the input image. Dilation (sometimes called "Minkowsky addition") is defined as follows.

$$A \oplus B = \{c \mid c = a + b \text{ for some } a \in A \text{ and } b \in B\} \quad (4)$$

Dilation works much like convolution: A kernel is slide to each position in the image and at each position "apply" (union) the kernel. In the case of morphology, this kernel B is called the structuring element. This is useful for decomposing a single large dilation into multiple smaller ones. Erosion which is sometimes called "Minkowsky subtraction" is defined as follows.

$$A \ominus B = \{x \mid x + b \in A \text{ for every } b \in B\} \quad (5)$$

Unlike dilation, erosion is not commutative. After edge detection, the edges of segments become some disconnected lines accompanied with interior gap. They should be connected to form the closed shapes by image dilation processing step. A few noisy edges can also be seen which are eliminated by image erosion processing step.

By using the above image processing methods, the features of loading areas can be extracted and loading surfaces are identified. The following demonstrates how edge detection is used. Image segmentation and binary morphology to identify loading of grinding wheel are described.

c	b	A
f	e	D
i	h	G

Fig. 3: Cartesian grid - eight neighbors for any point

-1	0	+1
-2	0	+2
-1	0	+1

(a) X-direction

+1	+2	+1
0	0	0
-1	-2	-1

(b) Y-direction

Fig. 4: unit vector specifying the derivative's direction

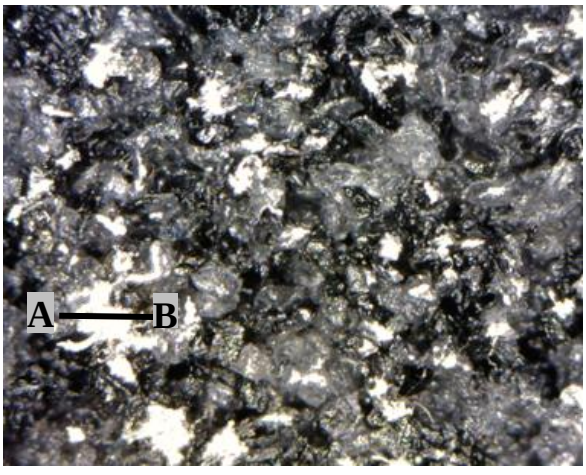

(a). Gray scaled Image

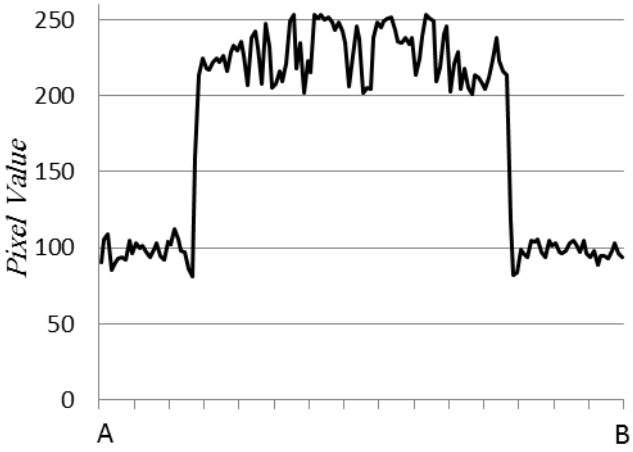

(b). histogram of intensity value along a line A-B.

Fig. 5: Pixel Values of Image

4. EXPERIMENTAL SETUP

The experiments were performed on a Hauni-Blum HFS204 Surface Grinder with a B126 N100 CBN vitrified wheel. Workpieces were nickel-base superalloy Inconel 738. A digital portable microscope Dino-Lite with adjustable magnification up to 230X was used to capture images of the wheel surface. The assembly is shown in Fig.6. Images were taken when the wheel was stationary. It consists of a positioning unit which traverses the microscope in direction of wheel width by a positioning unit driven via a stepper motor. The chips of grinding with CBN wheels are infinitesimal as compared with conventional wheels. For monitoring of CBN wheel loading, surface images should have large resolution and this causes the reduction of the field of view. This positioning unit assists in capturing images of full width of wheel. The axis of the microscope lens was perpendicular to the wheel surface. Microscope was equipped with adjustable LED ring light coaxial with the lens providing illumination.

Table 1: setup of parameters and specification of the grinding system

Machine	Model	*Hauni-Blohm HFS 204*
	Max. spindle speed	*4,000 rpm*
	Spindle power	*10 kW*
Dynamometer		*Kistler Type9255B*
Grinding Wheel		*1A1 200 10 B126 Vit. N V100*
Workpiece		*Inconel 738*
Table speed		*100mm/s*
Depth of Cut		*20 μm*
Cutting Speed		*30 m/s*
Length of stroke (*L*)		*50mm*
Coolant		*3% emulsion, 7.4 l/min*

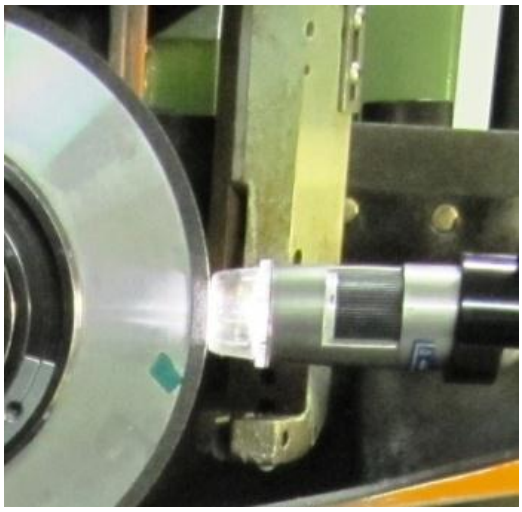

Fig. 6: The wheel loading measurement device

5. RESULTS AND DISCUSSION

The image processing technique applies disparity between optical characteristic of metal chip, abrasive grain and wheel bond. As it was discussed in the previous section, the range of light wavelength transparent to vitrified bond and also CBN grains is in the range of visible lights. This means they are relatively transparent to the visible and infrared light. The reflected light from metal chips on wheel surface is brighter than the bond and CBN grains. According to Fig. 1, the chip edges can be clearly distinguished from the pale wheel surface background. Black and amber-colored CBN grains, grey-colored vitrified bond can be seen in this figure. Loaded areas can also be distinguished in brighter color. The dark color of the edges of chips is attributable to the oxidation of chip materials. With the intention of decreasing the amount of computation in the process, gray scaled images were used. An M-file in Matlab was programmed to execute the discussed stages of image processing. To illustrate the process steps, Fig.7 presents an example which shows each stage separately. The converted original grayscale image can be seen in Fig. 7(a). Since image acquisition

may lead to noisy images, preprocessing operations are usually performed before edge detection. The most common preprocessing step in image processing applications is image normalization. Image normalization refers to eliminating image variations (such as noise, illumination, or occlusion) that are related to conditions of image acquisition and are unrelated to object identity.

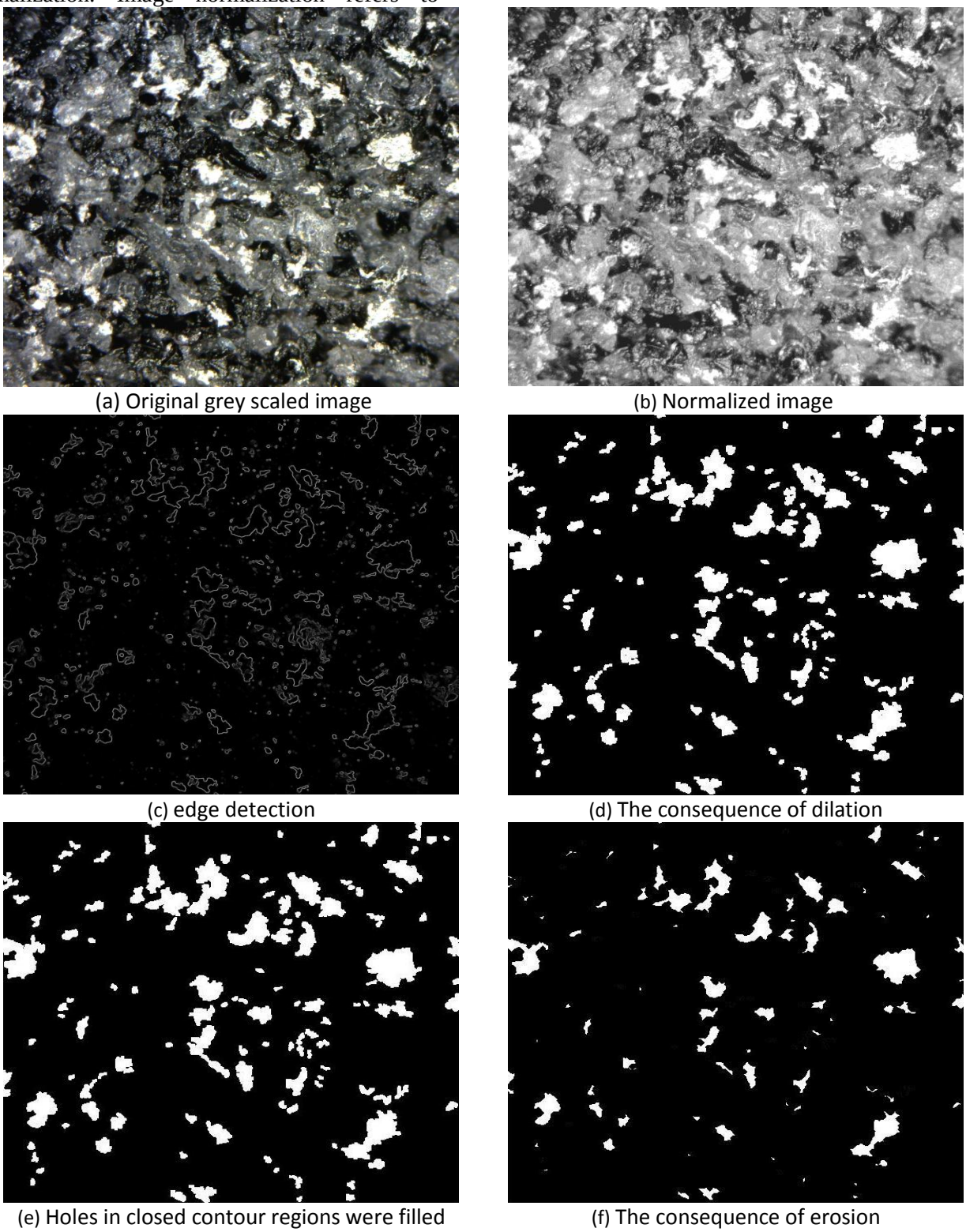

(a) Original grey scaled image

(b) Normalized image

(c) edge detection

(d) The consequence of dilation

(e) Holes in closed contour regions were filled

(f) The consequence of erosion

Fig.7: Steps of image processing of grinding wheel surface

The result of normalization of current example is shown in Fig. 7(b). Edge segmented image by Sobel operator can be seen in Fig. 7(c). Compared to the original image, gaps can be seen in the lines and areas surrounding the loading regions of the gradient mask. As discussed before, these gaps will disappear if the Sobel operated image is dilated. The consequence of dilation is shown in Fig. 7(d). The dilated gradient mask clearly shows the loaded regions, but there are still holes in the interior of the regions. To fill these holes any closed contour pixels in images should be filled as shown in Fig. 7(e). Finally, in order to make the segmented object look natural, the loaded areas were smoothened by eroding the image which the resulted image is shown in Fig. 7(f).

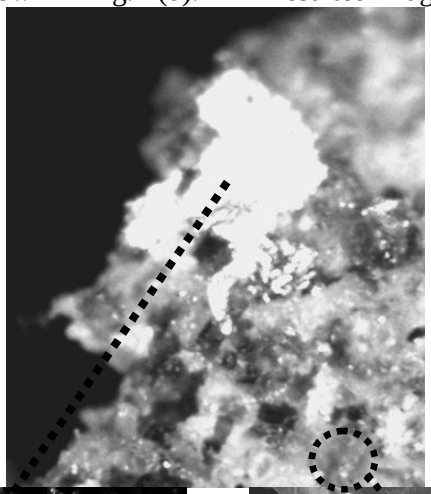

(a) Captured Image

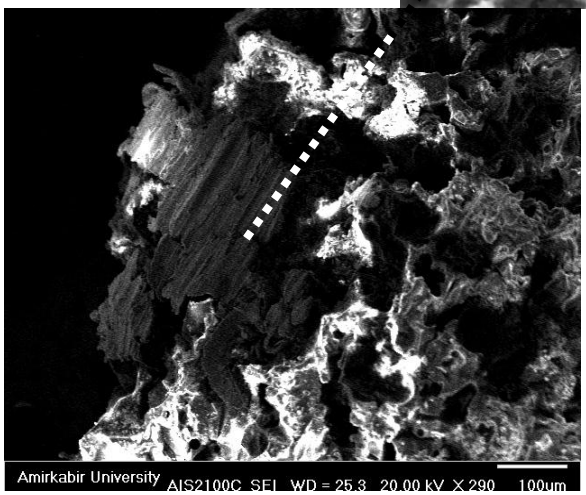

(b) SEM pictures of chip loaded area

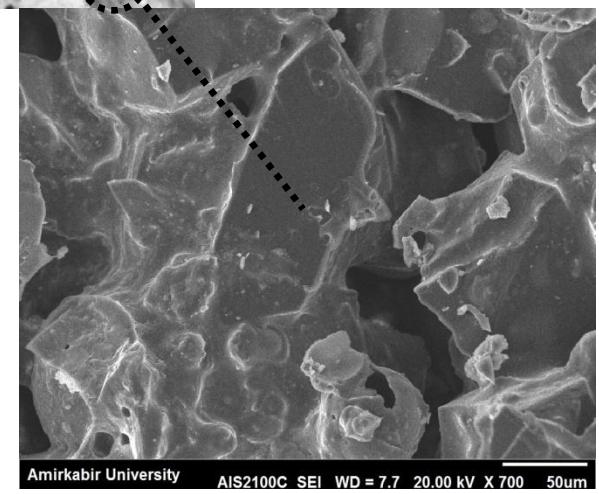

(c) SEM pictures of wear flat area

(d) Proccesed image

Fig. 8: Loaded areas compare with wear flat areas

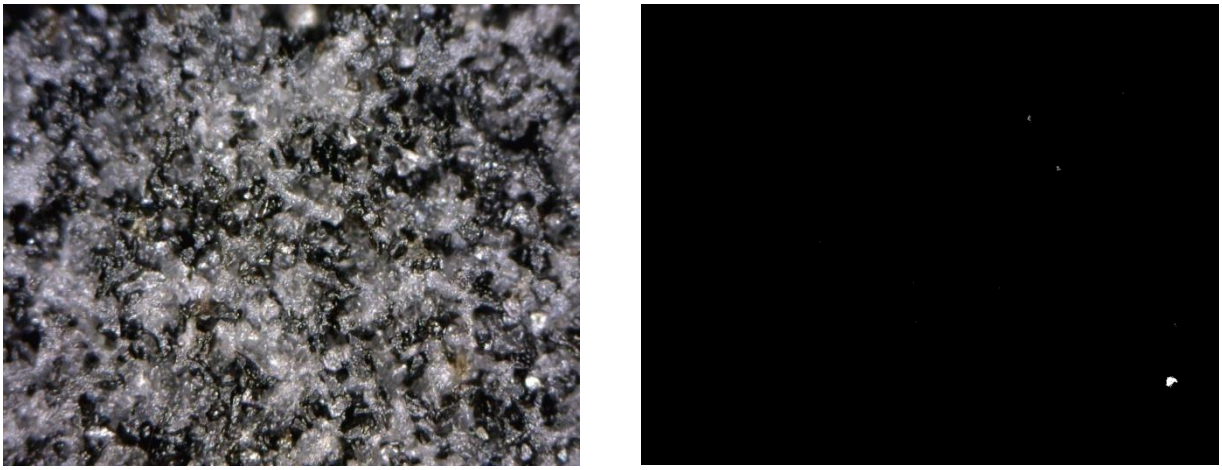

(a) newly dressed wheel surface (b) Processed image

Fig. 9: processing of newly dressed wheel surface image

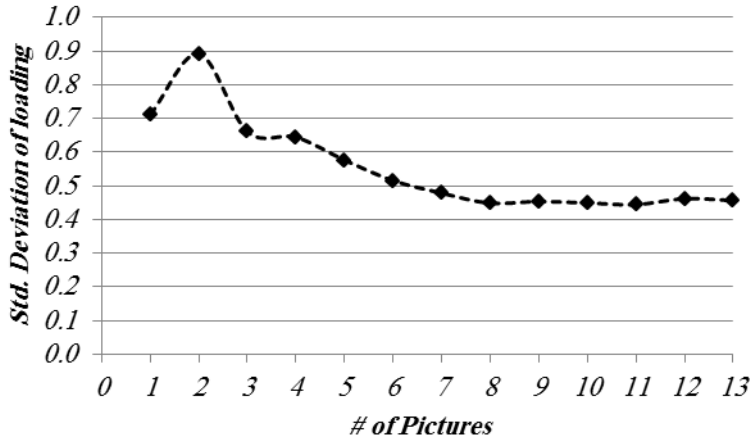

Fig 10: Standard deviation of loading percentage against number of pictures in circumference of wheel

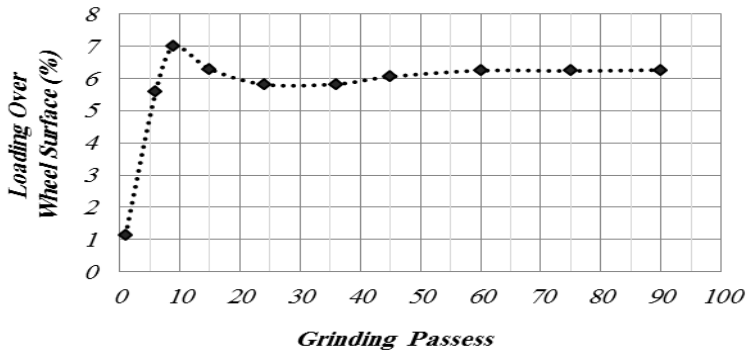

Fig. 11: Loading against grinding passes

The percentage of loaded area to wheel surface can be calculated simply by dividing the pixels numbers of area of interest to total pixel numbers. The percent of calculated loading chips on the wheel surface for this image is 4.93%. Owing to their uneven distribution, some grains attributed to wear flats are bright in the images which might be confused with the chips. Although, normalization eliminates this extremely high contrast points but these bright spots have wrong edge shapes and edge contrasts from different from that of the chips. Wear flats do not have dark edges but the

loaded areas have dark edges. By applying the iterative method for thresholding, high bright grain spots attributed to wear flats and also vitreous bond can be ruled out. To observe the wheel surface more clearly, a section of wheel surface was cut and was observed under SEM. As it can be seen in Fig. 8, CBN grains seem different from loaded chips. Figure 8(d) shows the processed image which does not include the wear flat area. This is due to different light reflected by CBN. The iterative method for determination of threshold value also eliminates the regions attributed to wear flats.

Figure (9) shows the image of a newly dressed wheel surface. Figure 9(a) is the original image and 9(b) is the processed gradient mask image. The ratio of loading of a fresh wheel surface is calculated to be 0.0604% in Fig. 9. The error is less than 0.1% which is acceptable in surface monitoring for grinding wheels.

To investigate the minimum number of pictures collected around the wheel circumference and reach steady state of the standard deviation of the loading percentage, grinding tests were carried out. Setup parameters and specification of the grinding system is presented in Table 1. Positioning assembly, as mentioned above, traverses the microscope in the width direction of the wheel. Four images in each circumferential location were captured to cover the full width. This process was done on several circumferential locations. Numbers of locations at wheel circumference ranging from three to thirteen were considered. Each image was processed and average standard deviations were calculated. In Figure 10 standard deviation of loading percentage against number of picture locations are plotted. After eight pictures in circumference of the wheel, standard deviation remained constant. Therefore eight locations from circumference and four images for each location across the width of the wheel were chosen to determine the amount of wheel loading.

To investigate the repeatability of the process, the average and standard deviation of loading percentage were calculated for different initial location of image capturing in the wheel circumference. The results are shown in Table. 2. A significant change is not seen for each condition. The steadiness of average value for more than eight numbers of pictures also shows good repeatability of the method.

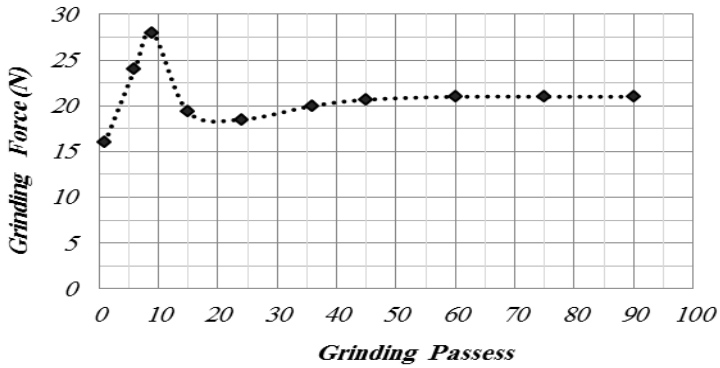

Fig. 12: Grinding force against grinding passes

Table 2: Average and Standard deviation for loading percent with different initial location point

Number of circumferential Locations	Initial Point 1			Initial Point 2			Initial Point 3		
	%L	Avr.	Std.	%L	Avr.	Std.	%L	Avr.	Std.
1	*5.80*	*5.80*	*0.71*	*7*	*7*	*0.51*	*6.45*	*6.45*	*0.05*
2	*7.05*	*6.43*	*0.89*	*6.3*	*6.65*	*0.54*	*5.90*	*6.18*	*0.60*
3	*6.79*	*6.55*	*0.66*	*5.7*	*6.33*	*0.68*	*7.00*	*6.45*	*0.55*
4	*5.90*	*6.39*	*0.64*	*5.9*	*6.23*	*0.65*	*5.95*	*6.33*	*0.55*
5	*6.80*	*6.47*	*0.58*	*6.8*	*6.34*	*0.58*	*6.50*	*6.36*	*0.48*
6	*6.50*	*6.47*	*0.52*	*6.45*	*6.36*	*0.52*	*6.42*	*6.37*	*0.43*
7	*6.30*	*6.45*	*0.48*	*6.9*	*6.44*	*0.51*	*6.80*	*6.43*	*0.41*
8	*6.70*	*6.48*	*0.45*	*6.83*	*6.49*	*0.49*	*6.89*	*6.49*	*0.41*
9	*7.00*	*6.54*	*0.45*	*6*	*6.43*	*0.49*	*6.80*	*6.52*	*0.40*
10	*6.10*	*6.49*	*0.45*	*7.1*	*6.5*	*0.5*	*6.00*	*6.47*	*0.41*

11	*6.91*	*6.53*	*0.44*	*6.2*	*6.47*	*0.48*	*6.60*	*6.48*	*0.39*
12	*5.90*	*6.48*	*0.46*	*6.87*	*6.5*	*0.48*	*6.20*	*6.46*	*0.38*
13	*6.90*	*6.51*	*0.46*	*6.35*	*6.49*	*0.46*	*7.00*	*6.50*	*0.39*
Average Value		*6.50*			*6.49*			*6.50*	

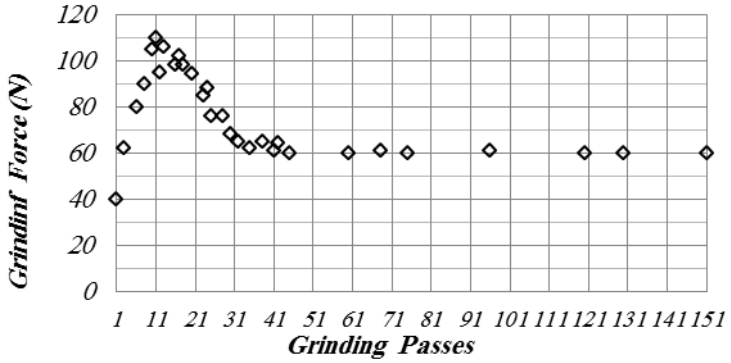

Fig. 13: Grinding force against grinding passes from results of P.Tso (1995)

For the performance of the image processing method, the amount of wheel loading against grinding passes is plotted in Fig. 11. As the grinding process continues and material removal volume increases, wheel loading increases. It was found that loading occurred rapidly at the beginning of a grinding experiment with a freshly dressed wheel. After the initial clogging, the progression of the loading occurred at a constant rate. As grinding goes on, the grinding force reaches high enough and chips are removed from the wheel surface. The bonding material and/or grains may also be removed. After a while, the loading percentage may settle down to a constant value. The measured tangential grinding force is plotted in Fig. 12. There is a good correlation between changes of wheel loading percentage which was measured by the presented technique with changes of grinding force. The same behavior is observed from results of P.Tso for CBN vitrified wheel as shown in Fig. 13 (Tso, 1995).

6. CONCLUSION

The measurement technique presented in this paper was applied by digital image processing for evaluation of wheel loading phenomena of a CBN vitrified grinding wheel. K-cluster iterative method was used to determine the threshold of edge detection. The accuracy of the method is reasonable and errors can be eliminated by the adjustment of bright grain spots. This can strongly decrease the noise of captured image. SEM observations showed the capability of the technique to detect the loaded area boundaries. This study provides the opportunity for the development of online grinding wheel monitoring using high speed camera.

REFERENCES

Al-Kindi GA, Shirinzadeh B (2007). An evaluation of surface roughness parameters measurement using vision-based data. International Journal of Machine Tools and Manufacture, (47): 697-708.

Bocquillon G, Loriers-Susse C, Loriers J (1993). Synthesis of cubic boron nitride using Mg and pure or M3-doped Li3N, Ca3N2 and Mg3N2 with M'=Al, B, Si, Ti. Journal of Materials Science, 28 (13): 35-47.

Cai R, Rowe WB, Morgan MN (2003). The Effect of Porosity on the Grinding Performance of Vitrified CBN. Key Engineering Materials, 238-239: 295-300.

Cameron A, Bauer R, Warkentin A (2010). An investigation of the effects of wheel-cleaning parameters in creep-feed grinding. International Journal of Machine Tools and Manufacture, 50 (1): 126-130.

Castejon M, Alegre E, Barreiro J, Hernandez L (2007). On-line tool wear monitoring using geometric descriptors from digital images. International Journal of Machine Tools and Manufacture, 47:. 1847-1853.

Dornfeld DA, Lee Y (2003). Chang, A. Monitoring of Ultraprecision Machining Processes. International Journal of Advanced Manufacturing and Technology, 21: 571–578.

Dou QP, Ma HT, Jia G, Chen ZG, Cao K, Ren C, Zhao JX, Liu XH, Zhang YH, Shi B, Zhang

TC (2006). Light emission from cBN crystal synthesized at high pressure and high temperature. Applied Physics Letters, id. 154102, 88(15).

Eremets MI, Gautheir M, Polian A, Chervin JC, Besson JM (1995). Optical properties of cubic boron nitride. PHYSICAL REVIEW B, The American Physical Society, 52: 8854-8863.

Feng Z, Chen X (2007). Image processing of grinding wheel surface. International Journal of Advanced Manufacturing Technology, 32: 27–33.

Gonzalez RC, Woods RE (2010). Digital Image Processing. Prentice Hall, 2010.

Haines J, Leger JM, Bocquillon G (2001). Synthesis and design of superhard materials. Annual Review of Materials Research, 31: 1.

Hosokawa A, Yasui H (2000). Characterization of the grinding wheel Surface by Means of Image Processing (1st report). JSPE, 62 (9): 1297–1301.

Kim SH, Ahn JH (1999). Decision of dressing interval and depth by the direct measurement. Journal of Materials Processing Technology, 1999, Vol. 88, pp. 190–194.

Konig W, Lauer-Schmaltz H (1978). Loading of the wheel phenomenon and measurement. Annals of the CIRP, 27: 217–220.

Lachance S, Bauer R, Warkentin A (2004). Application of region growing method to evaluate the surface condition of grinding wheels. International Journal of Machine Tools & Manufacture, 44(7-8): 823–829.

Lauer-Schmaltz, H. ; Konig, W. *Phenomenon of Wheel Loading Mechanisms in Grinding*. Annals of CIRP, 1980, Vol. 29, pp. 201-206.

Liu Q, Xun C, Nabil G (2007). Assessment of Al2O3 and superabrasive wheels in nickel-based alloy grinding. International Journal of Advanced Manufacturing Technology, 940–951.

Mao C, Zhou ZX, Ren YH, Zhang B (2010). Analysis and FEM Simulation of Temperature Field in Wet Surface Grinding, Materials and Manufacturing Processes, 25(6): 399-406.

Mersmann C (2011). Industrializing metrology—Machine vision integration in composites production. CIRP Annals - Manufacturing Technology, 60: 511-514.

Meyer F (1992). Color image segmentation. Maastricht, The Netherlands in Proc. Int. Conf. Image Processing, 303 – 306.

Mokbel AA, Maksoud TMA (2000). Monitoring of the condition of diamond grinding wheels using acoustic emission technique, Journal of Materials Processing Technology, 101(1–3): 292–297.

Nelson S A (2012). http://www.tulane.edu/~sanelson/geol211. [Online] Tulane University. [Cited: Feb. 16, 2012.]

Peatross J, Ware M (2011). Physics of Light and Optics. [ed.] C. online textbook.

Sakamoto H, Shimizu S, Kato D (1998). Evaluation of Loading Behavior of Grinding Wheel Based on Working Surface Topography. Journal of the Japan Society of Precision Engineering, 64(9): 1320-1324.

Li S, Lijie C, Hao L, et al. (2010). Large Scale Growth and Characterization of Atomic Hexagonal Boron Nitride Layers. NanoLett, 10 (8): 3209–3215.

Srivastava AK, Ram KS, Lal GK (1985). A new technique for evaluating wheel loading. International Journal of Machine Tools Des. & Res., 25: 33-38.

Teichera U, Künanz K, Ghosh A, Chattopadhyay AB (2008). Performance of Diamond and CBN Single-Layered Grinding Wheels in Grinding Titanium, Materials and Manufacturing Processes, 23(3).

Tso PL (1995). Study on the grinding of Inconel 718. Journal of Materials Processing Technology, 55: 421-426.

Wei J, Zhang Q, Xu Z, Lyu (2010). Study on precision grinding of screw rotors using CBN wheel, International Journal of Precision Engineering and Manufacturing International Journal of Precision Engineering and Manufacturing, 11 (5): 651-658.

Yasui H, Hiraki Y, Sakata M (2001). Development of Automatic Image Processing System for Grinding Wheel Surface. J. Japan society for prec. Eng., 67.

Zhong Z, Hung NP (2000). Diamond Turning and Grinding of Aluminum-Based Metal Matrix Composites, Materials and Manufacturing Processes , Volume 15(6): 853-865.

Zhong Z, Ramesh K, Yeo SH (2010). Grinding of nickel-based supper-alloys and advances ceramics, Materials and Manufacturing Processes, 16 (2): 195-207.